Article

Not peer-reviewed version

Efficient Decellularization of Full-Thickness Rat Derived Abdominal Wall to Produce Acellular Biologic Scaffolds for Tissue Reconstruction: Promising Evidence Acquired From in vitro Results

George Skepastianos , Panagiotis Mallis * , Epameinondas Kostopoulos , Efstathios Michalopoulos , Vasileios Skepastianos , Chrysoula Palazi , Lucia Pannuto , Gerasimos Tsourouflis

Posted Date: 7 July 2023

doi: 10.20944/preprints202307.0478.v1

Keywords: Abdominal wall; decellularization; hernia; tissue reconstruction; biomechanical analysis; full-thickness abdominal wall scaffold

Article

Efficient Decellularization of Full-Thickness Rat Derived Abdominal Wall to Produce Acellular Biologic Scaffolds for Tissue Reconstruction: Promising Evidence Acquired from In Vitro Results

George Skepastianos [1,2,†], Panagiotis Mallis [2,*,†], Epameinondas Kostopoulos [1], Efstathios Michalopoulos [2], Vasileios Spepastianos [1], Chrysoula Palazi [1], Lucia Pannuto [4] and Gerasimos Tsourouflis [5]

[1] Plastic Surgery Department, EANP Metaxa, National Hospital of Athens, 51 Botatsi Street, 185 37 Pireus, Greece; skep-19@hotmail.com (G.S.); epamkostop67@hotmail.com (E.K.); bskepastianos@hotmail.com (V.S.); xrisa.pal@gmail.com (C.P.)
[2] Center of Experimental Surgery, Biomedical Research Foundation Academy of Athens, 4 Soranou Ephessiou Street, 115 27 Athens, Greece; pmallis@bioacademy.gr (P.M.); smichal@bioacademy.gr (E.M.)
[3] Hellenic Cord Blood Bank, Biomedical Research Foundation Academy of Athens, 4 Soranou Ephessiou Street, 115 27 Athens, Greece
[4] Queen Victoria Hospital NHS Foundation Trust, East Grinstead RH19 3DZ, UK; lucia.pannuto@gmail.com (L.P.)
[5] Second Department of Propedeutic Surgery, Medical School, University of Athens, 11527 Athens, Greece; gerasimos.ts@gmail.com (G.T.)
* Correspondence: pmallis@bioacademy.gr; Tel.: +306971616467
† Equally contributed to this work as first authors.

Abstract: Background: Functional restoration of abdominal wall defects represent one of the fundamental challenges of reconstructive surgery. Synthetic grafts or crosslinked animal-derived biological grafts are characterized by significant adverse reactions, which are mostly observed after their implantation. The aim of this study was to evaluate the efficacy of the decellularization protocol to produce a completely acellular full-thickness abdominal wall scaffold. Methods: Full-thickness abdominal wall samples were harvested from Wistar rats and submitted to a 3 cylce decellularization process. Histological, biochemical and DNA quantification analyses were applied to evaluate the effect of the decellularization protocol. Mechanical testing and immunogenicity assessment were also performed. Results: Histological, biochemical and DNA analysis results showed the efficient decellularization abdominal wall samples after the 3rd cycle. Decellularized abdominal wall scaffolds were characterized by good biochemical and mechanical properties. Conclusion: The data presented herein confirm the effective production of rat-derived full-thickness abdominal wall scaffold. Expanding this approach will allow the exploitation of the capacity of the proposed decellularization protocol in producing acellular abdominal wall scaffolds from larger animal models or human cadaveric donors. In this way, the utility of biological scaffolds with preserved in vivo remodelling properties may be one step closer to its application in clinical studies.

Keywords: Abdominal wall; decellularization; hernia; tissue reconstruction; biomechanical analysis; full-thickness abdominal wall scaffold

1. Introduction

The restoration of abdominal wall defects as a result of occurred trauma, infection, congenital conditions, complications of abdominal surgeries, neoplastic diseases and others belongs among the most routinely performed surgeries of the general population [1]. Beneath them, incisional hernias that occurred after laparotomy, are exhibited in 5-20% of patients, and their repair represents a highly

 doi:10.20944/preprints202307.0478.v1

demanding reconstructive surgery [2]. It is estimated that more than 700.000 surgeries for abdominal wall reconstruction are performed in the United States, annually and more than 20 million are performed globally, each year [1–4].

Mostly, abdominal wall surgery and herniation can lead to significant complications including muscle weakness and collagen ratio disturbance [5]. Regarding the latter, it has been already described in the literature, that the amount of collagen I is reduced, while the amount of collagen III is increased, resulting in alterations in abdominal wall tensile strength and mechanical stability [5–8]. In accordance with the above-provided information, the proper reconstruction of abdominal wall defects requires the use of scaffolds characterized by specific biomechanical properties, to support tissue regeneration and deep wound healing [9]. Nowadays, a great number of commercially produced synthetic scaffolds are used as implants for abdominal wall reconstruction [1,10,11]. Synthetic scaffolds can be produced utilizing either biodegradable or non-biodegradable materials. Polyglycolic acid (PLGA) and polyglactin 910 (PLGA 910), are biodegradable materials, which are degraded through the hydrolysis process [12–14]. In this way, tissue-resident macrophages can efficiently degrade these materials into monomers, which further can be deposited to the regenerated ECM. However, the abdominal wall reconstruction performed with biodegradable materials results mostly in scar tissue formation at the injury site [15–17]. This in turn can result in complications due to scar tissue formation, impairing in this way tissue integrity and mechanical resistance. Unfortunately, new reconstructive surgery to replace the formed scar tissue is required [18]. On the other hand, polypropylene (PP) and expanded tetrapolyfluorethylene (ePTFE) belong to the category of non-biodegradable materials, with good biomechanical properties and tissue reinforcement [19–21]. Although these materials have good properties, severe adverse reactions such as calcification, and host immune system activation have been reported in the majority of the cases [1].

For this purpose, scaffolds derived from different origins e.g. natural plant-based or animal-derived ECM must be evaluated as a potential new strategy for abdominal wall reconstruction. In the context of tissue regeneration, biological scaffolds composed of native or glutaraldehyde crosslinked ECM, have been used in the past, with limited success [22,23]. However, after long-term implantation, also aberrant host immune responses have been reported [24,25]. Immune system activation includes mostly the polarization of macrophages into the M1 phenotype, the activation of CD4 T cells, and the migration of Th1 and B cells to the implantation site, which further leads to calcification and tissue rejection [24–26]. On the other hand, the production of biological scaffolds utilizing advanced tissue engineering approaches such as decellularization may overpass the aforementioned issues [27]. Decellularization relies on the use of a combination of physical and chemical methods, leading to cellular loss and the production of an acellular matrix [28]. The decellularized ECM can beneficially support cell adhesion, survival, proliferation, and differentiation, compared to the synthetic or cross-linked scaffolds [29]. The latter is related also to better biomechanical properties, which can lead to improved tissue reconstruction at the injury site [30,31]. Currently, different research groups elaborate on protocols for the successful decellularization of abdominal wall scaffolds of animal origin [32–34]. The application of decellularization protocol can be easily performed in a great variety of tissues, although the preservation of the full-thickness ECM, comprises a highly demanding task. For this reason, the literature regarding the successful production of full-thickness abdominal wall scaffolds is limited [32–34], yet the needs of reconstructive surgery demand the production of such structures. In the past, perfusion decellularization was proposed for the production of whole organ scaffolds, however, this process is laborious and requires advanced equipment and well-trained personnel [35]. Although, the broad use of the above method, still serious issues concerning extensive ECM or capillary network damage, have been already reported, which may lead to unfavourable results regarding tissue implantation and cell repopulation either under *in vitro* or *in vivo* conditions [32–34]. Based on our previous experience, we have validated a cost-effective perfusion-free decellularization method, which can potentially be applied as an alternative method for the production of full-thickness abdominal wall scaffolds [33].

 doi:10.20944/preprints202307.0478.v1

The aim of this study was to test the efficacy of the production of an acellular scaffold originating from full-thickness rat-derived abdominal wall samples. For this purpose, our optimized decellularization protocol consisting of 3 cycles, was applied to a full-thickness rat-derived abdominal wall. The evaluation of the decellularized abdominal wall ECM was performed using methods such as histological analysis, biochemical and DNA quantification. Furthermore, the biomechanical properties of the abdominal wall before and after the decellularization approach were also investigated. The obtained results may lead to significant conclusions regarding the full-thickness abdominal wall decellularization, to be used in large-scale experimental procedures.

2. Methods

2.1. Abdominal Wall Excision

Whole abdominal walls were harvested from Wistar rats (n=30), weighing 300-400 gr, under aseptic conditions. All animals were provided by the Animal Facility of the Biomedical Research Foundation Academy of Athens (BRFAA). Well-trained personnel of the animal facility handled and cared for the animals according to the international guidelines of animal care, and conformed with the Helsinki Declaration. In addition, this study was approved by the Bioethics Committee of BRFAA (ref 02-2021). Briefly, the animals were euthanatized and using sterile instruments a paramedian incision in the anterior abdominal wall was performed, in order to expose the external oblique muscles. The abdominal wall samples were extracted in dimensions of 4 x 5 cm and then stored in Phosphate Buffer Saline (PBS, Sigma-Aldrich, Darmstadt, Germany) 1x supplemented with 1% Penicillin-Streptomycin (P-S, Sigma-Aldrich, Darmstadt, Germany), until further processing.

2.2. Decellularization of whole rat abdominal wall samples

Whole abdominal wall samples (n=30) were decellularized using an already published protocol, validated previously in our lab [33]. Whole rat abdominal wall samples were incubated with decellularization buffers under vigorous agitation at 150 rpm. The decellularization procedure involved the incubation of the samples in CHAPS buffer, pH:7 (8 mM CHAPS, 1 M NaCl and 25 mM EDTA, in PBS 1x, Sigma-Aldrich, Darmstadt, Germany) for 18 h at room temperature (RT), followed by subsequent incubation in SDS buffer, pH:7 (1.8 mM SDS, 1 M NaCl and 25 mM EDTA, in PBS 1x, Sigma-Aldrich, Darmstadt, Germany) for another 18h at RT. Finally, the samples were placed in a solution containing a-Minimum Essentials Medium (a-MEM, Sigma-Aldrich, Darmstadt, Germany) supplemented with 40% v/v Fetal Bovine Serum (FBS, Gibco, Thermo Fisher Scientific, Waltham, MA, USA) for 36 h at 37^{o} C. After each decellularization buffer, 3x washes with PBS 1x (Sigma-Aldrich, Darmstadt, Germany), at RT was performed. The whole decellularization procedure was repeated another 2 times (in total 3 decellularization cycles, n=5 samples/decellularization cycle).

2.3. Histological Analysis

Non-decellularized (n=10) and decellularized (n=15) whole rat abdominal wall samples (obtained from the 1st, 2nd and 3rd decellularization cycle) were fixed overnight using the 10% v/v neutral formalin buffer (Sigma-Aldrich, Darmstadt, Germany), followed by washes with distilled water. After this step, all samples were dehydrated in an increasing series of alcohol buffers, paraffin-embedded and finally sectioned at 5 μm. The production of acellular abdominal wall scaffolds was evaluated with the performance of specific histological stains. For this purpose, hematoxylin and eosin (H&E, VWR, Avantor, Radnor, PA, USA), Sirius Red (SR, VWR, Avantor, Radnor, PA, USA), Orcein (OS, VWR, Avantor, Radnor, PA, USA) and Toluidine Blue (TB, VWR, Avantor, Radnor, PA, USA) were used for the evaluation of abdominal wall ECM, collagen fibers, elastin fibers and sulphated glycosaminoglycans (sGAGs), respectively. The sections of non-decellularized and decellularized abdominal wall samples were deparaffinized, rehydrated, stained with each stain, and mounted with a cover slide. Whole rat abdominal wall samples were characterized by a combination of longitudinally and circumferentially oriented fibers, and for this purpose, representative images were obtained. Images were acquired using the Leica DM L2 light microscope (Leica Microsystems,

 doi:10.20944/preprints202307.0478.v1

Weltzar, Germany) and processed with Image J v.1.46 (Wane Rasband, National Institute of Health, Bethesda, USA).

To further evaluate the impact of each decellularization cycle on collagen type I, indirect immunofluorescence was performed. Briefly, the sections of all study samples were deparaffinized, rehydrated, and blocked. Then, incubation with the primary monoclonal antibody against collagen type I (1:1000, Sigma-Aldrich, Darmstadt, Germany), was performed. Brief washes were performed and then incubation with the FITC-conjugated IgG secondary antibody (1:500, Sigma-Aldrich, Darmstadt, Germany) was performed. Finally, cell nuclei were stained with DAPI (Sigma-Aldrich, Darmstadt, Germany), and then the samples were dehydrated, and glycerin mounted. The samples were examined under the LEICA SP5 II confocal microscope and representative images were acquired with the LAS Suite v2 software (Leica Microsystems, Weltzar, Germany).

2.4. Biochemical analysis

The biochemical analysis included the evaluation of collagen (hydroxyproline) and sGAGs content. Moreover, representative areas of non-decellularized and decellularized whole rat abdominal wall samples (1 x 1 cm) were selected from each sample. Specifically, for the collagen content quantification, non-decellularized (n=10) and decellularized (n=30, n=10 / decellularization cycle) were digested in papain solution (125 μg / ml, Sigma-Aldrich, Darmstadt, Germany) at 60^{o}C for 10, or until full digestion of the samples. Collagen content was estimated based on the determined hydroxyproline content with the hydroxyproline assay kit (MAK008, Sigma-Aldrich, Darmstadt, Germany) following the manufacturer's instructions. SGAGs content in non-decellularized (n=10) and decellularized (n=30, n=10 / decellularization cycle) was performed, as has been previously described. Briefly, the samples were digested with 1 ml of lysis buffer (0.1 M Tris pH:8, 0.2 M NaCl and 5 mM EDTA in PBS 1x (Sigma Aldrich, Darmstadt, Germany) and 25 mg/ml proteinase K (Sigma-Aldrich, Darmstadt, Germany) at 56^{o}C for 12 h. Inactivation of proteinase K was performed at 95^{o}C, for 5 min. The 1% w/v dimethylene blue stain (Sigma-Aldrich, Darmstadt, Germany) was used and the determination of sGAG content of each sample was performed photometrically at 525 nm. Finally, the sGAG concentration of each sample was estimated through interpolation to a standard curve, based on chondroitin sulphate standards of 3, 6, 12, 25, 50, 100 and 150 μg / ml.

2.5. DNA quantification

For the DNA quantification, non-decellularized (n=10) and decellularized (n=30, n=10 / decellularization cycle) samples, were initially digested using a Proteinase K (25 μg / ml, Sigma-Aldrich, Darmstadt, Germany) in PBS 1x (Sigma-Aldrich, Darmstadt, Germany) at 56^{o} C for 12 h, followed by inactivation at 96^{o}C for 5 min. Then, isolation of DNA of each sample was performed and finally eluted in 50 μl RNAse free water (Sigma-Aldrich, Darmstadt, Germany). The DNA content of each sample was spectrophotometrically determined using the Nanodrop (Thermo Fischer Scientific, Waltham, Massachusetts, USA) at 260 / 280 nm. Also, the DNA quantification results were verified using DNA electrophoresis on 1% w/v agarose gel. Images were acquired with the UVITEC Imaging System (Cleaver, Scientific, Warwickshire, USA).

2.6. Biomechanical Analysis

Biomechanical analysis of non-decellularized (n=5) and decellularized (n=5/ cycle) whole rat abdominal wall samples was performed to evaluate the mechanical properties. The biomechanical analysis involved the uniaxial testing of the samples which was performed in a Zwick/Roell tensile tester (model Z 0.5, Zwick GmbH & Co. KG, Ulm, Germany) equipped with a 100 N load cell. Non-decellularized and decellularized samples were cut into longitudinal strips (l=40 mm, w=10 mm) and placed before the analysis in prewarmed Krebs-Ringers (Gibco, Thermo Fisher Scientific, Waltham, MA, USA) solution (at 37^{o}C). During the biomechanical testing, the strips were continuously sprayed with PBS 1x (Sigma-Aldrich, Darmstadt, Germany). The strips derived from non-decellularized and decellularized samples were clamped at their ends, with sandpaper to avoid sample slippage, under

 doi:10.20944/preprints202307.0478.v1

zero strain on the mechanical device, which produced a preloading value of 0.005 N, before the data collection. All samples were preconditioned for 10 cycles at a rate of 10 mm/min. Sample extension (Δl, in mm) accompanying the generated load (F, in Newtons) were converted to engineering strain (ε), and engineering stress (σ in MPa). Elastin (El-E) and collagen (Col-E) phase slope, transition stress (σTrans) and strain (εTrans), ultimate tensile strength (σUTS) and failure strain (εUTS) were used, to analyze the stress-strain behaviour of the studied samples.

2.7. Determination of Acellular Whole Abdominal Wall Immunogenicity

To determine the immunogenicity of decellularized whole abdominal wall scaffolds, the following assays were performed. Indirect immunofluorescence against α-gal (1:500, Sigma-Aldrich, Darmstadt, Germany) and collagen type I (1:1000, Sigma-Aldrich, Darmstadt, Germany) was performed as has been previously described. Secondary PE-conjugated monoclonal antibody (1:50) against α-gal epitope and FITC-conjugated monoclonal antibody (1:500) against collagen type I were used for the detection of the aforementioned proteins. Finally, all samples were dehydrated, glycerin mounted and examined using the LEICA SP5 II confocal microscope coupled with the LAS Suite v2 software (Leica Microsystems, Weltzar, Germany). In addition, the detection of α-gal epitopes was performed using the ELISA method, for additional verification of indirect immunofluorescence results. Initially, non-decellularized (n=5) and decellularized samples (n=5 / each cycle) were fully lysed in a 1% w/v papain medium (Sigma-Aldrich, Darmstadt, Germany) at 37° C for a maximum of 10 hours. Then, the occurred lysates passed through 0.25 nm filters. After this step, the ELISA method was performed, following the manufacturer's instructions (ab239716, Abcam, Cambridge, United Kingdom). Furthermore, gene expression profile in non-decellularized and decellularized samples was performed. Total mRNA was isolated from non-decellularized (n=5) and decellularized (n=5 / each cycle) using the TRI-reagent (Sigma-Aldrich, Darmstadt, Germany) according to the manufacturer's instructions. The concentration of isolated mRNA was photometrically determined. Then, at least 400 ng of total mRNA was used as template for the cDNA production using the Omniscript reverse transcription kit (Qiagen, Hilden, Germany). PCR was performed using the Taq PCR master mix (Cat No 201443, Qiagen, Hilden, Germany) on Biometra T Gradient Thermoblock PCR Thermocycler (Biometra, Gottingen, Germany) with a final volume of 25 μl for each PCR reaction. The PCR program involved the below steps: 1) denaturation at 95°C for 15 min, 2) denaturation at 94° C for 30 s, 3) annealing at 60-62° C for 90 s and 4) extension at 72° C for 3 min. The number of cycles used in this program was 35. The primer pairs for each PCR reaction are listed in Table 1. Finally, the PCR products were analyzed with electrophoresis on agarose gel (1% w / v, Sigma-Aldrich, Darmstadt, Germany). In addition, to evaluate the immunogenicity of non-decellularized and decellularized abdominal wall samples, flow cytometric analysis was also performed. Initially, non-decellularized (n=5) and decellularized samples (n=5 / each cycle) were fully digested in a 1% w/v collagenase medium at 37° C for a maximum of 4 hours. The isolated cells were washed 3 times with PBS 1x (Sigma-Aldrich, Darmstadt, Germany) and then were submitted for the flow cytometric analysis. Specifically, cells obtained from all samples were analyzed for the expression of RT1 class I, RT1 class II, CD31 and a-SMA. Monoclonal antibodies against RT1 Class I, and a-SMA and a-SMA, were conjugated with fluorescein isothiocyanate (FITC), while RT1 class II and CD31 were conjugated with phycoerythrin (PE) and Peridinin-Chlorophyll-protein (PERCP), respectively. Anti-RT1 class I and class I were purchased from Biocompare (South San Francisco, USA). The rest of the monoclonal antibodies were purchased from BD Biosciences (New Jersey, USA) and analyzed at a minimum of 10000 all events in FACS Calibur (BD Biosciences, New Jersey, USA).

Preprints (www.preprints.org) | NOT PEER-REVIEWED | Posted: 7 July 2023 doi:10.20944/preprints202307.0478.v1

Table 1. Primer pairs for the PCR reactions.

Gene	Gene ID	Forward Primer	Reverse Primer	Amplicon size
RT1 Class I	309627	CAGATCCCCCAAAGGCACAT	CAGATCCCCCAAAGGCACAT	253
RT1 Class II	309622	CTTCCTTACCCGGGTGGAAC	TCTGATCACGAGCCGTATGC	316
Gapdh	24383	GGCCCGGAGTCTAAAGTAGC	GGCGGCCAGTTACCATAAGT	234

2.8. Statistical Analysis

The statistical analysis of this study was performed using GraphPad Prism v 6.01 (GraphPad Software, San Diego, CA, USA). Comparisons regarding the hydroxyproline, sGAG, DNA content and also comprehensive biomechanical analysis were performed using the Kruskal-Wallis test. Furthermore, validation of our results involved the use of the unpaired nonparametric Mann-Whitney U test. Statistically significant differences between group values were considered when p value was less than 0.05. Indicated values were presented as mean ± standard deviation.

3. Results

3.1. Histological and biochemical evaluation of decellularized whole rat-derived abdominal wall.

To properly evaluate the decellularization process of full-thickness rat-derived abdominal wall, histological and biochemical analyses, was initially performed. The abdominal wall represents a complex tissue including a combination of circumferential and longitudinal fibers, and for this purpose, the histological analysis involved the evaluation of both axes. A total number of 3 decellularization cycles was required for the efficient production of acellular whole abdominal wall scaffolds. By the end of the 3rd decellularization cycle, the acellular whole abdominal wall scaffold appeared translucent, indicating furthermore the proper elimination of the resident cellular populations (Figure 1).

In addition, the ECM integrity of the decellularized abdominal wall scaffold was retained properly among all layers of the tissue (Figure 1 and Figure 2). No cracks or other destruction evidence were observed in the produced decellularized whole rat abdominal wall scaffold (Figure 1 and Figure 2). To assess better the decellularization efficacy, H&E stain was initially performed. The removal of the resident cells was initially observed after the 1st decellularization cycle, however, total cell and nuclear material elimination was detected by the end of the 3rd decellularization cycle (Figure 2). Once the cell elimination was confirmed by the H&E staining, further evidence regarding the ECM composition of the acellular whole abdominal wall scaffold was provided after the performance of Orcein stain, Sirius Red, and Toluidine blue. Moreover, Sirius red staining revealed the preservation of the collagen fibers both in circumferential and longitudinal directions in the decellularized abdominal wall scaffolds. No destruction or change in the collagen fibers alignment was detected between native and decellularized abdominal wall scaffolds (after the 3rd cycle). On the other hand, the abdominal wall is characterized by the presence of low elastin amount, and in our case was difficult to be detected with the performance of Orcein stain, however, no significant change was observed between non-decellularized and decellularized abdominal wall samples (after the 3rd cycle). On the other hand, sGAGs in the decellularized abdominal wall appeared to be affected by each decellularization cycle (Figure 2). Indeed, after the accomplishment of each decellularization cycle, the Toluidine blue stain (specifically stains the sGAGs) was weaker. Finally, the produced acellular full-thickness abdominal wall scaffolds (after the 3rd cycle) characterized by a significant loss of sGAGs, as it was indicated by the Toluidine blue stain.

Preprints (www.preprints.org) | NOT PEER-REVIEWED | Posted: 7 July 2023 doi:10.20944/preprints202307.0478.v1

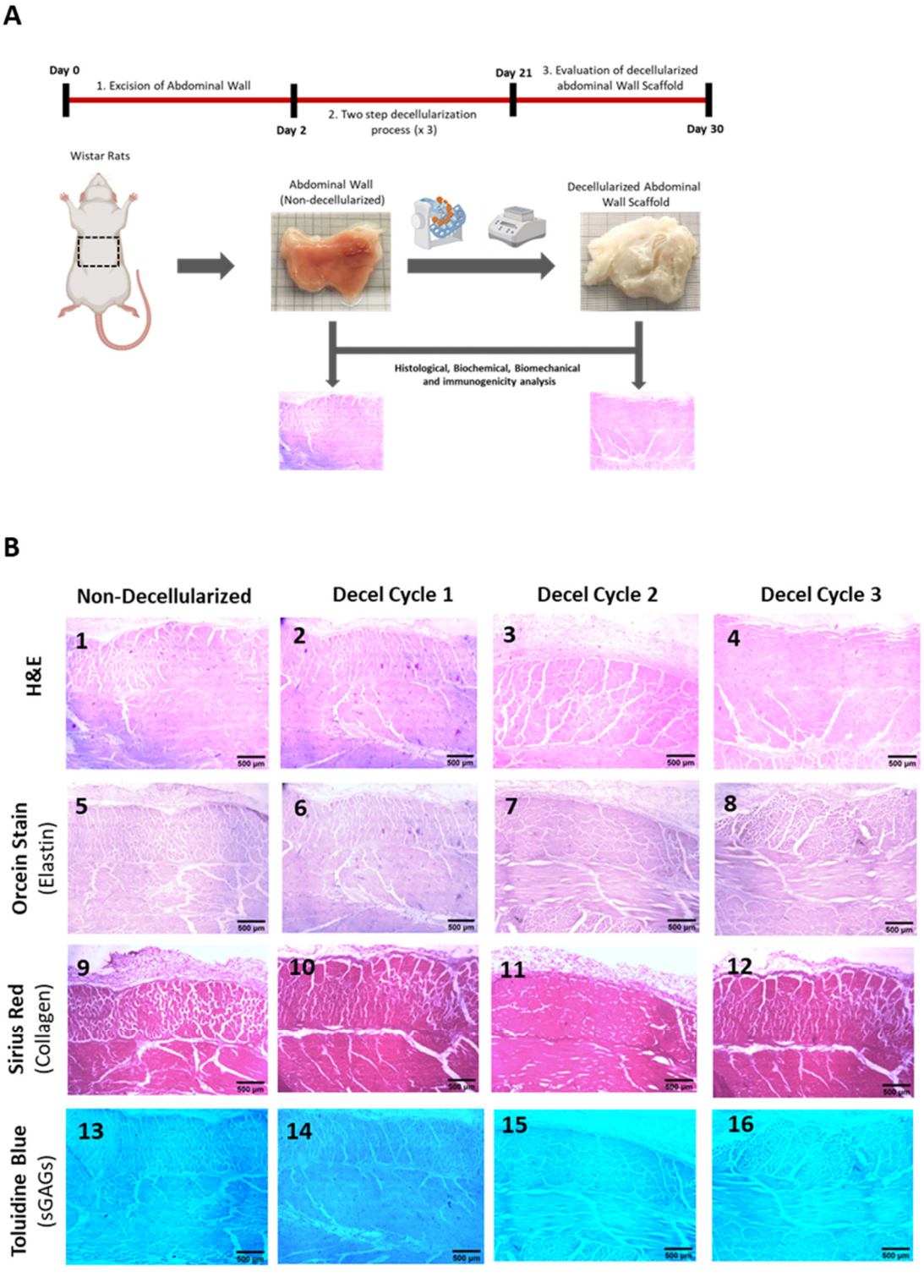

Figure 1. Assessment of decellularization of the full-thickness rat-derived abdominal wall. Overview of the applied decellularization protocol for producing acellular full-thickness abdominal wall scaffolds (A). Histological analysis involving the performance of H&E (B1–B4), Orcein stain (B5–B8), Sirius red (B9–B12) and Tolouidine blue (B13–B16) of non-decellularizaed and decellularized full-thickness abdominal wall samples. All images are presented with original magnification 2.5x and scale bars 500 μm.

Preprints (www.preprints.org) | NOT PEER-REVIEWED | Posted: 7 July 2023 doi:10.20944/preprints202307.0478.v1

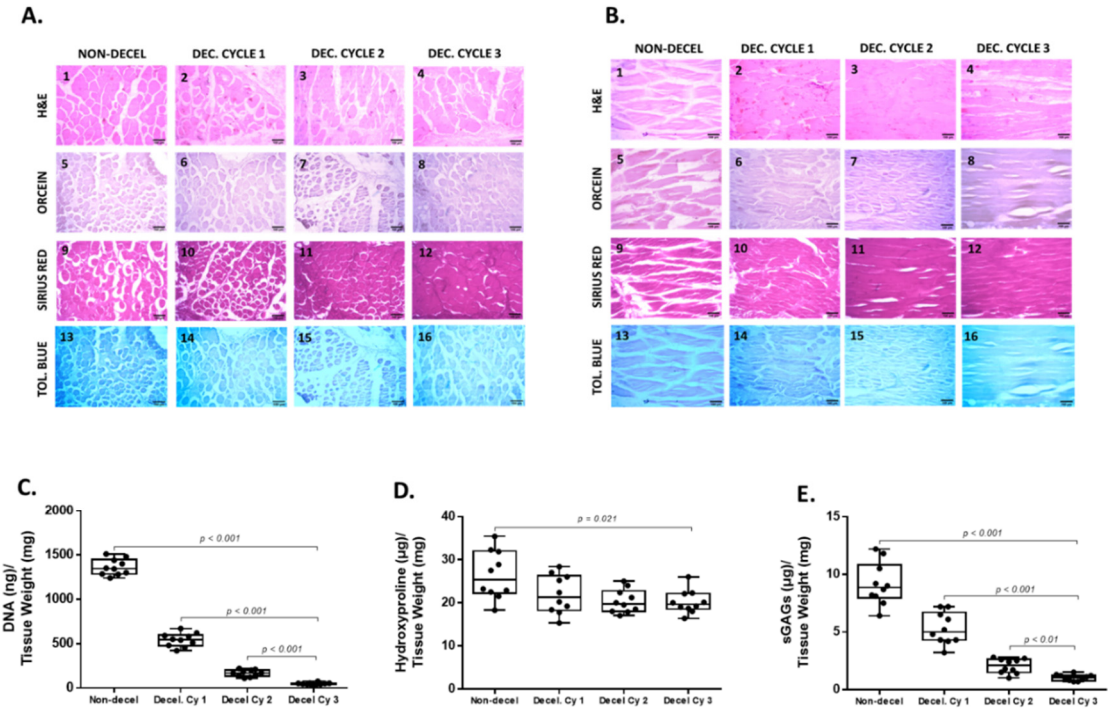

Figure 2. Evaluation of the decellularization approach for producing acellular whole rat abdominal wall scaffolds using histological and biochemical approaches. Representable images of non-decellularized and decellularized samples stained with H&E in circumferential (A1–A4) and longitudinal (B1–B4) axis. Hematoxylin stain was only evident in non-decellularized samples, which further confirmed the presence of cell nuclei. No hematoxylin stain was weaker after each decellularization cycle. Decellularized samples after the 3rd cycle were characterized by the absence of hematoxylin stain, thus confirming further the removal of cellular materials. No alteration in orcein stain between non-decellularized and decellularized samples was observed either in the circumferential (A5–A8) or longitudinal (B5–B8) axis. Collagen fibers appeared to be retained both in composition and alignment as has been indicated by Sirius red statin either in circumferential (A9–A12) or longitudinal (B9-B12) axis. Representable images of non-decellularized and decellularized samples stained with Toluidine blue, either in the circumferential (A13–A16) or longitudinal (B13–B16) axis. The staining intensity of Toluidine blue became weaker after each decellularization cycle, compared to the non-decellularized samples, indicating the removal of the sGAGs. All images were presented with original magnification 10x, and scale bars 100 μm. DNA quantification (C) and biochemical analysis including the determination of the hydroxyproline content (D) and sGAG content (E) were performed to validate further the decellularization process. Statistically significant differences regarding the DNA content ($p< 0.001$), hydroxyproline content ($p= 0.021$) and sGAGs ($p <0.001$) were observed between non-decellularized and decellularized samples.

DNA quantification and biochemical analyses were performed to validate further the composition of the decellularized whole rat abdominal wall. Specifically, the DNA content after the performance of each decellularization cycle was statistically significantly reduced ($p < 0.001$). Non-decellularized samples contained 1363 ± 87 ng DNA/mg dry tissue weight (Figure 2), while the DNA content of decellularized samples was 542 ± 73, 167 ± 35 and 48 ± 12 ng DNA / mg dry tissue weight after the 1st, 2nd and 3rd cycles, respectively. The hydroxyproline content, which corresponds to collagen, was reduced statistically significantly ($p = 0.021$) in decellularized samples. The hydroxyproline content of non-decellularized samples was 26 ± 5 μg / mg dry tissue weight. The hydroxyproline content of decellularized samples after the 1st, 2nd and 3rd cycles was 22 ± 4, 20 ± 3 and 20 ± 2 μg hydroxyproline/mg dry tissue weight, respectively (Figure 2). The sGAG content of non-

 doi:10.20944/preprints202307.0478.v1

decellularized samples was 9 ± 2 μg sGAGs / mg dry tissue weight, while decellularized samples had 5.3 ± 1.7, 2.1 ± 0.6 and 1.1 ± 0.3 μg sGAGs / mg dry tissue weight, respectively (Figure 1). Statistically significant difference was observed in sGAGs content between non-decellularized and decellularized samples of the whole abdominal wall ($p < 0.001$). In addition, indirect immunofluorescence against collagen type I in combination with DAPI stain was performed to validate further the decellularization process. The results of indirect immunofluorescence showed the preservation of the collagen type I in decellularized whole abdominal wall scaffolds (after the 1st, 2nd and 3rd cycles) in both axes. On the other hand, DAPI stain which was specific for the cell nuclei gradually lost its intensity signal after the 1st decellularization cycle (Figure 3). To confirm these results, the determination of MFI of collagen type I and DAPI stain was performed in all samples. In the circumferential axis, non-decellularized and decellularized samples after 1st, the 2nd and 3rd cycles were characterized by 80.3 ± 3.5, 81.2 ± 3.8, 80.3 ± 2.6 and 80.7 ± 2.1 MFI, for collagen type I and 72.1 ± 6.8, 30.4 ± 7.1, 11.7 ± 4.4 and 1.1 ± 0.3 for DAPI stain, respectively (Figure 3). In the longitudinal axis, the MFI of non-decellularized and decellularized samples after the 1st, 2nd and 3rd cycle was 81.4 ± 7.7, 80.6 ± 3.4, 80.7 ± 2.4 and 80.6 ± 2.3 for collagen type I and 73.7 ± 4.7, 27.3 ± 4.1, 9.7 ± 3.1 and 0.9 ± 0.3 for DAPI stain, respectively (Figure 3). Statistically significant differences were observed between the study samples only for the DAPI stain in both axes ($p < 0.001$).

3.2. Evaluation of biomechanical properties

The evaluation of the decellularization process for the production of acellular whole abdominal wall scaffolds involved the uniaxial testing of non-decellularized and decellularized samples (after 1st, 2nd and 3rd cycles, Figure 4). Specifically, the σ_{Trans} for the non-decellularized and decellularized samples of 1st, 2nd and 3rd cycles were 105 ± 15, 184 ± 15, 208 ± 25 and 218 ± 28 kPa, respectively (Figure 4). The ε_{Trans} for the non-decellularized and decellularized samples of 1st, 2nd and 3rd cycles was 309 ± 20, 312 ± 47, 312 ± 45 and 313 ± 36, respectively (Figure 4). The σ_{UTS} for the non-decellularized and decellularized samples of 1st, 2nd and 3rd cycles was 899 ± 51, 1026 ± 107, 1028 ± 160 and 1035 ± 136 kPa (Figure 4). The ε_{UTS} for the non-decellularized and decellularized samples of 1st, 2nd and 3rd cycles was 681 ± 66, 859 ± 98, 860 ± 55 and 916 ± 160 (Figure 4). The El-E for the non-decellularized and decellularized samples of 1st, 2nd and 3rd cycles was 88.2 ± 8, 101 ±16, 113 ± 22 and 115 ± 14 kPa (Figure 4). The Col-E for the non-decellularized and decellularized samples of 1st, 2nd and 3rd cycles was 2840 ± 352, 3139 ± 375, 3156 ± 377 and 3161 ± 444 kPa, respectively (Figure 4). Statistically significant differences regarding the σ_{Trans} ($p< 0.001$), ε_{UTS} ($p< 0.01$) and El-E ($p< 0.001$), were observed between non-decellularized and decellularized samples.

3.3. Evaluation of Immunogenicity on decellularized whole abdominal wall scaffolds

To further evaluate the immunogenicity of non-decellularized and decellularized abdominal wall scaffolds, the detection of α-gal epitopes utilizing the indirect immunofluorescence approach was performed. A-gal epitopes were successfully detected in non-decellularized and decellularized samples after the 1st and 2nd cycles (Figure 5). On the other hand, no presence of α-gal was detected in decellularized samples after the 3rd cycle (Figure 5). Furthermore, quantification of α-gal with the ELISA method was performed to further verify the indirect immunofluorescence results. Interestingly the concentration of α-gal in non-decellularized samples was 763 ± 67 pg / μl, while in decellularized samples after the 1st , 2nd and 3rd cycles was 591 ± 45, 122 ± 21 and 25 ± 11 pg / μl, respectively (Figure 5). Statistically significant difference regarding the presence of α-gal was observed between non-decellularized and decellularized samples ($p< 0.001$).

Preprints (www.preprints.org) | NOT PEER-REVIEWED | Posted: 7 July 2023 doi:10.20944/preprints202307.0478.v1

Moreover, to detect, total mRNA was extracted from non-decellularized and decellularized samples, reversely transcribed and the occurred cDNA was used for the determination of *RT1 class I/ II* and *Gapdh*. Detection of *RT1 class I/ II* and *Gapdh* was only detected in non-decellularized and decellularized samples after the 1st cycle. No expression of the aforementioned genes was detected in decellularized abdominal wall scaffolds after the 2nd and 3rd cycles (Figure 5). Further verification of these results, was achieved using the flow cytometric approach against RT1 CLASS I/ II, CD31 and A-SMA. Specifically, the detected expression for the previously mentioned molecules was above 95 % for the non-decellularized samples and more than 93% for the decellularized samples after the 1st cycle. On the other hand, the expression of RT1 CLASS I /II, CD31 and a-SMA was below 1% for the decellularized abdominal wall scaffolds after the performance of the 2nd and the 3rd cycles (Figure 5).

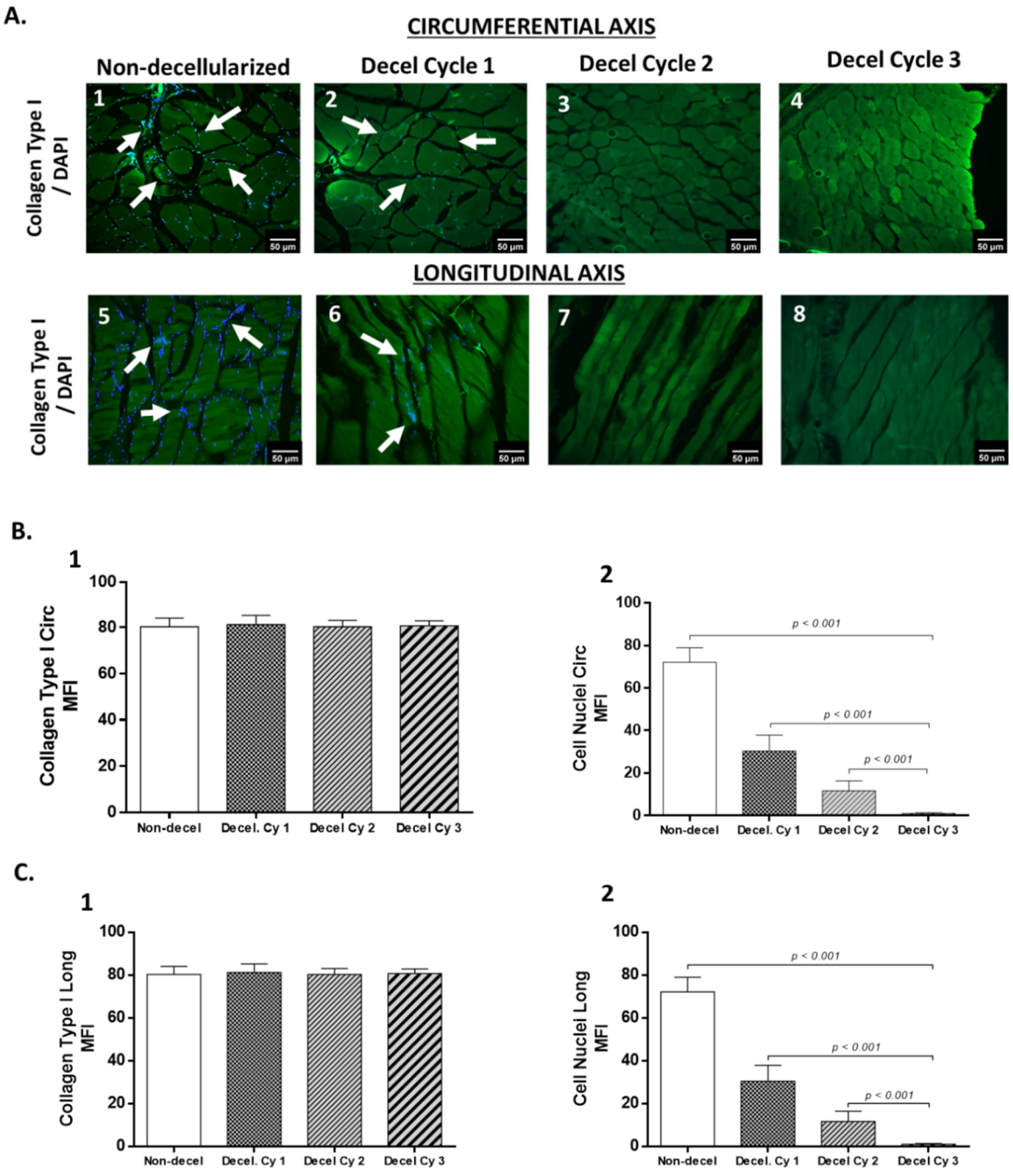

Figure 3. Evaluation of the decellularized whole abdominal wall scaffolds with the indirect immunofluorescence. Indirect immunofluorescence against collagen type I (green) in combination with DAPI stain (blue), was applied both in non-decellularized and decellularized whole abdominal

Preprints (www.preprints.org) | NOT PEER-REVIEWED | Posted: 7 July 2023 doi:10.20944/preprints202307.0478.v1

wall scaffolds (after the 1st, 2nd and 3rd cycle, circumferential and longitudinal axes, A1-A8). White arrows indicated the presence of cell nuclei. Cell nuclei were evident in non-decellularized and decellularized samples after the 1st cycle. No cell nuclei were detected in decellularized samples after the 2nd and 3rd decellularization cycles in both axes. The images were presented with original magnification of 20x, and scale bars 50 μm. MFI of detected collagen and DAPI stain of all samples in both circumferential and longitudinal axis was determined as shown in graphs B1, B2 and C1, C2. Statistically significant differences were observed between non-decellularized and decellularized samples regarding the DAPI stain both in the circumferential ($p< 0.001$) and longitudinal ($p < 0.001$) axis.

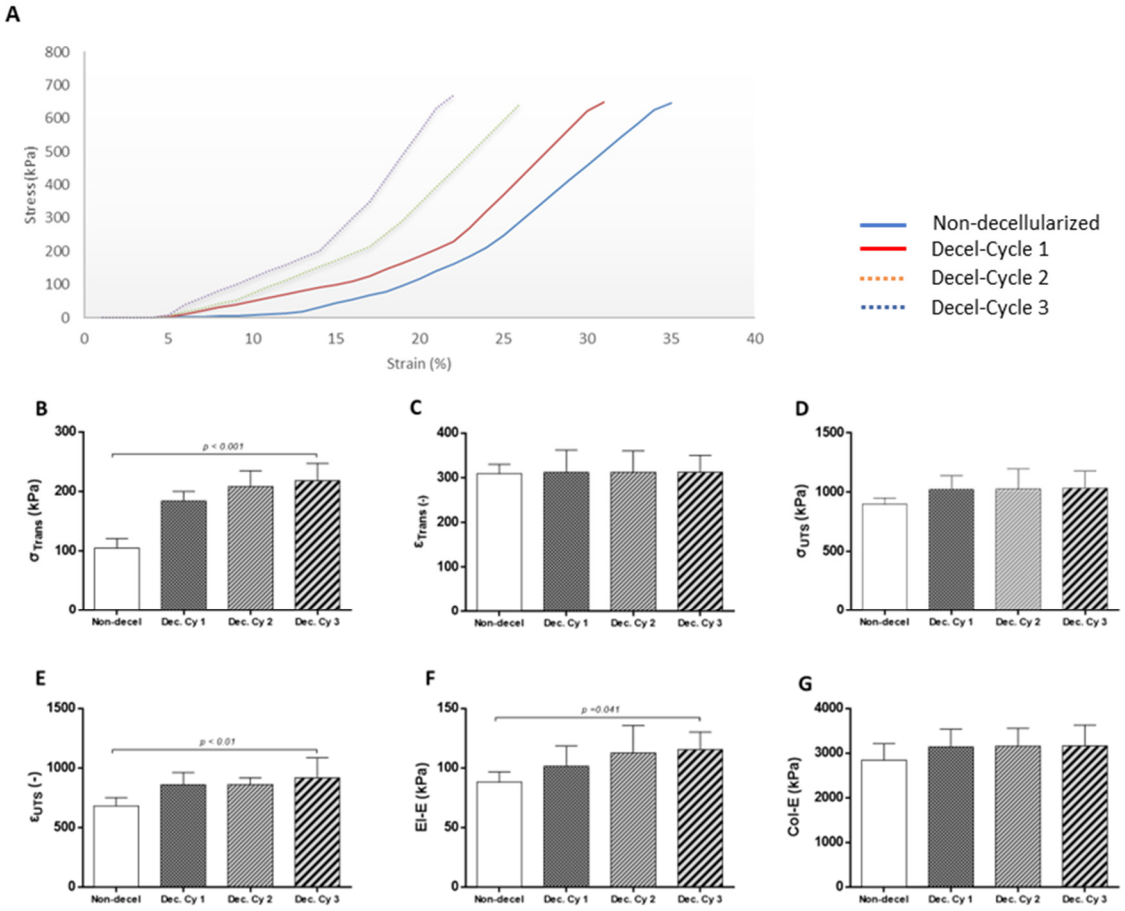

Figure 4. Biomechanical evaluation of non-decellularized and decellularized whole abdominal wall scaffolds. Representative stress-strain curves of non-decellularized and decellularized samples after the performance of 1st, 2nd and 3rd cycles. The biomechanical analysis involved the determination of σTrans (B), εTrans (C), σUTS (D), εUTS (E), El-E (F) and Col-E (G). Statistically significant differences were observed only for the σTrans ($p< 0.001$), εUTS ($p< 0.01$) and El-E ($p< 0.001$), between non-decellularized and decellularized samples.

Preprints (www.preprints.org) | NOT PEER-REVIEWED | Posted: 7 July 2023 doi:10.20944/preprints202307.0478.v1

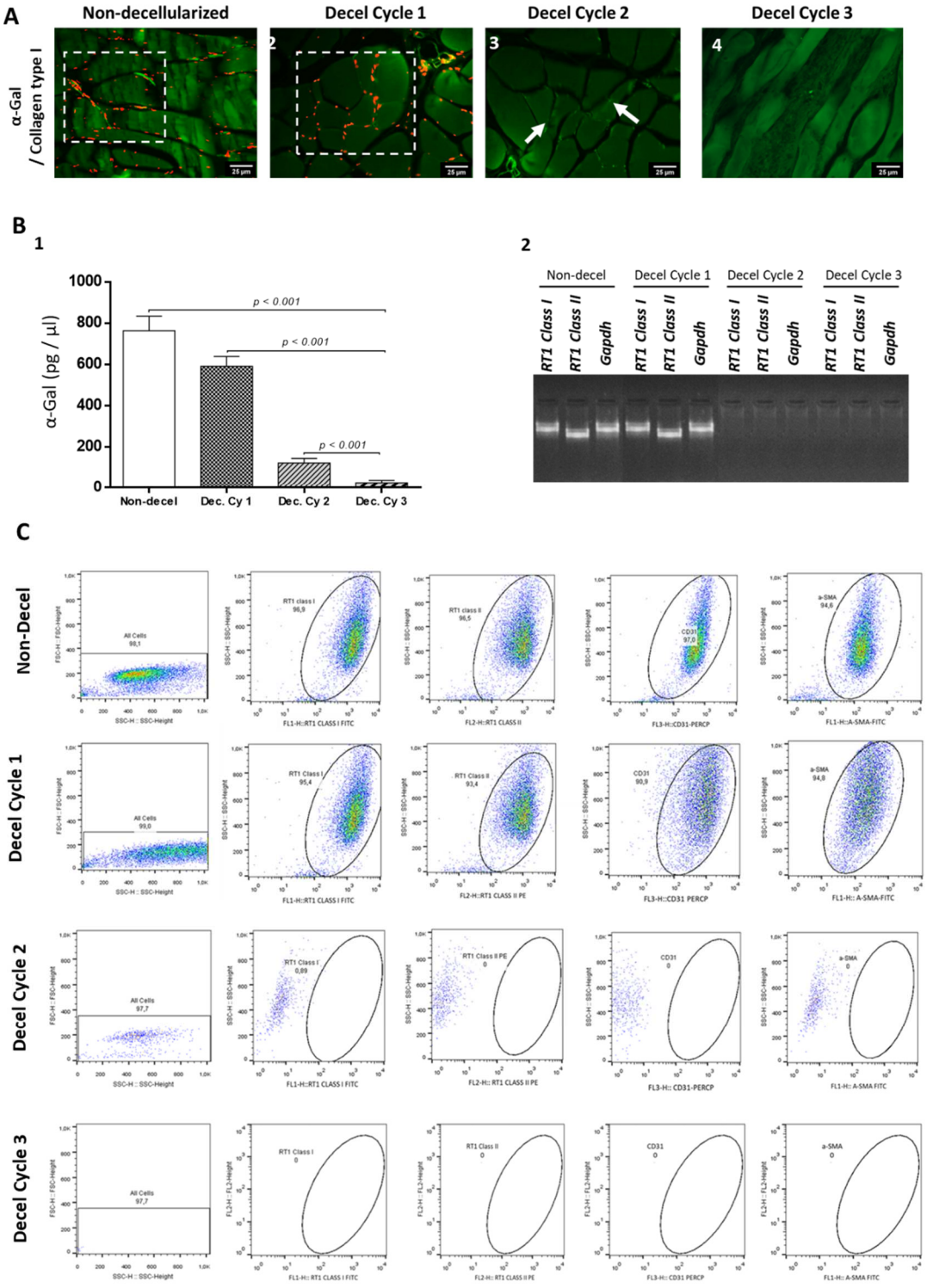

Figure 5. Evaluation of whole abdominal wall immunogenicity before and after the complete decellularization procedure. Indirect immunofluorescence against α-gal and collagen type I of non-decellularized (A1) and decellularized after the 1st (A2), 2nd (A3) and 3rd (A4) decellularization cycles. White boxes and arrows indicated the presence of α-gal in abdominal wall samples. No presence of α-gal signal was detected in decellularized whole abdominal wall scaffolds after the performance of the 3rd cycle. Images presented with original magnification 40x and scale bars 25 µm. Detection of α-gal epitope in non-decellularized and decellularized abdominal wall samples using the ELISA method (B1). Statistically significant difference was observed regarding the α-gal expression among

 doi:10.20944/preprints202307.0478.v1

all samples ($p< 0.001$). DNA electrophoresis in agarose gel 1% v/v regarding the expression of *RT1 class I, RT1 class II* and *Gapdh* in non-decellularized and decellularized samples (B2). No detection of the PCR products *RT1 class I, RT1 class II* and *Gapdh* was observed in decellularized samples after the 2nd cycle. Quantification of α-gal in non-decellularized and decellularized samples after the 1st, 2nd and 3rd decellularization cycles (B2). Statistically significant difference regarding the α-gal was found between native and decellularized samples ($p< 0.001$). Flow cytometric analysis of RT1 Class I, RT1 Class II, CD31 and α-SMA in non-decellularized and decellularized samples.

4. Discussion

In the field of reconstructive surgery, the use of the appropriate prosthetics for the restoration of abdominal wall defects represents one of the greatest challenges of the last decade. Currently, a great number of biomaterials have been used for abdominal wall reconstruction, however, both synthetic biodegradable and non-biodegradable scaffolds are accompanied by severe adverse reactions such as scar tissue formation, altered mechanical properties, calcification and eventually graft loss [1,10–21]. Recently, animal-derived crosslinked biological scaffolds are also considered as an alternative and promising solution, for the proper restoration of abdominal wall defects [22,23]. Nevertheless, their natural origin crosslinked biological scaffolds are characterized by calcification occurrence and M1 macrophage-mediated tissue rejection [24,25]. More than 20 million abdominal wall reconstructive surgeries are performed annually at the international level, and for this reason, the search and utilization of alternative abdominal wall meshes, are highly important [1–4]. Taking into consideration the above data, the application of a non-immunogenic biological scaffold utilizing state-of-the-art tissue engineering methods for abdominal wall defect restoration may represent a promising alternative source of transplants. The present study aimed to the production of full-thickness abdominal wall scaffolds, utilizing a validated decellularization approach. For this purpose, rat-derived abdominal wall samples were decellularized appropriately to produce acellular non-immunogenic biological scaffolds, to serve as potential grafts for future abdominal wall tissue restoration. Initially, full-thickness abdominal wall samples were harvested, washed to remove any blood clots and submitted immediately to decellularization. Histological analysis revealed that complete decellularization of full-thickness abdominal wall scaffolds was achieved after the accomplishment of the 3rd cycle. Cell removal was initiated after the 1st decellularization cycle, however complete cell and nuclear remnants were eliminated by the end of the proposed protocol. In addition, decellularized abdominal wall scaffolds (after the 3rd decellularization cycle) were characterized by the preservation of collagen, a significant ECM component. On the other hand, sGAGs appeared to be significantly removed after the application of the decellularization protocol. Regarding the elastin content, besides its low presence in the abdominal wall, no significant alteration between non-decellularized and decellularized samples was observed. The preservation of collagen in decellularized samples was further confirmed by the performance of indirect immunofluorescence (against collagen type I in combination with DAPI). Moreover, collagen type I fibers in decellularized samples retained their alignment both in the circumferential and longitudinal axis in the same way as the non-decellularized samples. The preservation of collagen type I in decellularized samples is of significant importance, comprising one of the major proteins of ECM structure, thus contributing to a great number of processes such as hemostasis performance and regulation of the wound healing process of the injured area [38]. Besides its function in tissue healing, collagen type I plays a significant role in the recruitment and attachment of specific cellular populations to the wounded region through binding to arginine-glycine-aspartic acid (RGD) binding motifs [39–44]. Indeed, various cellular populations such as fibroblasts, pericytes and mesenchymal stromal cells can bind to the collagen fibers through the interaction of α1β1, α2β1 and $\alpha\nu\beta$1 with the RGD binding motifs of well-aligned collagen fibers, thus further can promote the wound healing and tissue regeneration [39–44]. Specifically, it has been shown that integrin-mediated binding with the RGD motifs can lead to an important intracellular signalling cascade through the upregulation of ILK-NF-kb, and GSK3β-AP1-CyclinD1, promoting in this way the cell survival, migration and proliferation to the injured site [39–46]. Besides, the collagen fibers also sGAGs are playing important role in collagen fibers

 doi:10.20944/preprints202307.0478.v1

orientation, and their loss after the decellularization process may affect the ECM structure and mechanical properties of the occurred scaffold [47,48]. However, the results of the present study seem to be in accordance with previously performed works, where also significant differences in sGAGs content were observed in decellularized samples. Importantly, in the study of Luo *et al.* [49] and Gui *et al.* [50] the levels of sGAG content in decellularized heart valves and umbilical arteries, respectively, were lower compared to the non-decellularized tissues. This can be explained by the already knowledge of the anionic nature of SDS, which is used as a basic detergent in all these studies [28]. SDS can interfere with the negatively charged sites of the sGAGs, and thus can efficiently remove them from the decellularized tissue [28,49].

The above results regarding the collagen, sGAGs and cell removal were also confirmed by the quantification assays performed in the present study. Importantly, the cell removal was further confirmed by the low levels of the isolated DNA content from decellularized samples. Indeed, the performance of each decellularization cycle appeared to be lower compared to the previous one. Finally, after the 3rd decellularization cycle, the DNA concentration was below 50 ng / μl dry tissue, thus confirming further the criteria for successful tissue decellularization as have been outlined by Gilbert *et al.* [28], and Crapo *et al.* [51]. In the present study, the DNA concentration was determined, through the measurement of 260 nm / 280 nm ratio with a spectrophotometer, avoiding in this way false quantification results occurring using commercial kits such as the Picogreen assay. Most of these commercial kits determine only the double-stranded (ds) DNA, without measuring the single-stranded (SS) DNA, which also may be present, especially in decellularized tissues [49,52]. Using the spectrophotometer, the genetic material quantification is most accurate, representing better the DNA content of the decellularized tissues. It is also widely known, that both ds and ss DNA can initiate a specialized immune response against the implanted graft, which could result in significant adverse reactions to the host [49,52,53].

Biomechanical properties are playing important role in tissue mechanics and therefore were evaluated before and after the decellularization process applied to the full-thickness abdominal wall scaffolds. Interestingly, decellularized abdominal wall scaffolds characterized by higher values of σ_{Trans}, ε_{Trans}, σ_{UTS}, ε_{UTS}, El-E and Col-E compared to the non-decellularized samples, suggesting the adaptation of a stiffer behavior by the produced scaffolds. Also, it was observed that differences in biomechanical properties were observed after the performance of each decellularization cycle. Overall, the increase in abdominal wall scaffold strength is respective to the ECM structure. Considering that the collagen fibers are responsible for the preservation of tissue integrity during occurred overload differences in the corresponding anatomical area, changes in collagen orientation play important role in altered mechanical properties of the produced scaffolds. In addition, decellularized abdominal wall scaffolds were characterized by greater extensibility than the non-decellularized samples, which is further related to the disorganized collagen fibers alignment. To assess the relationship between the ECM structure and biomechanical properties, extensive histological analysis of all study samples both in circumferential and longitudinal directions was performed in the present study. However, histological analysis results did not reveal any change in the collagen fibers orientation (in both axis). Moreover, the indirect immunofluorescence results against collagen type I confirmed further the results obtained from the histological stains, thus confirming the preservation of collagen fibers alignment after the performance of the decellularization procedure. Besides collagen fibers, also elastin fibers are playing important role in tissue mechanical strength and extensibility. However, the elastin content in the abdominal wall is relatively low and the elastin fibers are mostly disorganized compared to other tissues such as elastic vessels (e.g. thoracic or abdominal aorta). However, no change in elastin content was observed between non-decellularized and decellularized abdominal wall samples. The explanation regarding the stiffer behavior of the decellularized scaffolds may be attributed to the cellular population elimination in the produced scaffolds. Indeed, SMCs and ECs, besides their important role in other biological processes, have the ability to retain the orientation of the collagen fibers, thus contributing further to the preservation of the ECM integrity. Based on the histological analysis, the collagen fibers of the non-decellularized samples are fully crimped, while in scaffolds are becoming uncrimp after

the performance of each decellularization cycle. To this phenomenon, also the reduction of the sGAG content observed in decellularized scaffolds may play its role in the collagen crimp. It is known, that sGAGs are forming large polymers called proteoglycans which actively contribute to collagen cross-linking [54]. The significant reduction of sGAGs in combination with the cellular elimination may lead to an important change in collagen crosslink, thus affecting further their crimp. Similar alterations in biomechanical properties have also been revealed in the past in other structures such as the aorta, intestine and elastic vessels, and have been extensively reported by Sexton *et. al.* [55], Stehbens *et. al.* [56], Sokolis *et. al.* [57] and Stergiopoulos *et. al.* [58]. Specifically, Stergiopoulos *et. al.* [58] indicated in their model, that the alteration of the biomechanical properties acquired by the decellularized scaffolds cannot be the mere result of cellular elimination only, but further structural ECM changes may provoke altered mechanical behavior. In a similar way, there is substantial evidence for the physical link between SMCs, ECs and ECM components, which further may contribute to the existence of residual forces in the abdominal wall. On the other hand, decellularization cause alterations at both the structural and cellular levels of ECM, thus the prestressed fibers no longer exist, and this may be the explanatory cause of the stiffer behavior of the decellularized abdominal wall scaffolds. Besides the above evidence for the altered mechanical properties explanation, stiffer abdominal wall scaffolds have been observed in other studies conducted with similar preparation methods. Specifically, Sanchez *et. al.* [32], Buell *et. al.* [33] and Chiu *et. al.* [34] demonstrated decellularized abdominal wall constructs with similar biomechanical properties, as those presented herein.

The immunogenicity of the decellularized scaffolds constitutes another important parameter, to serve as potential biological grafts. To assess if the proposed decelluarization protocol could be submitted for the preparation of acellular scaffolds of animal origin, the determination of α-gal epitopes was performed. Complete elimination of α-gal epitope was achieved after the performance of the 3rd decellularization cycle, as it was indicated by histological and quantification analysis results. A-gal epitopes are considered as main immunogenic antigens and related to hyper-acute rejection when xeno-transplantation was performed in the past [59–61]. Currently, there is a great amount of performing efforts to produce α-Gal epitope free knockout pigs, which can offer a solution to a global shortage of organs, however, this attempt is costly [62,63]. In the context of biological scaffold production originating from animal models, the decellularization method could potentially assist with this issue. The SDS, a detergent of decellularization, is known for its ability to break the hydrophobic interactions, and ionic and hydrogen bonds, thus can successfully remove negatively charged proteins and genetic material. In such a way, SDS has been shown that potential may interfere with the α-gal epitopes, forcing their elimination by the tissue's ECM. Although efforts in removing animal-derived antigens from biological scaffolds were performed, α-Gal epitopes have been found in transplants such as heart valves, SIS-ECM and vessel grafts, impairing the graft longevity after transplantation [59–66]. In the present study, the proposed decellularization protocol successfully eliminated the α-gal epitopes from the produced scaffolds, thus decreasing their potential immunogenicity upon implantation [64–66]. Moreover, molecular and cytometry analysis revealed the absence of both cellular populations e.g. ECs and SMCs and other antigenic epitopes e.g. the *RT1 class I* and *II*. RT1 class I and class II comprise the analogue genes of histocompatibility in rats [67,68]. Histocompatibility antigens are actively implicated in transplantation and graft survival, and their removal may be related to the production of universal biological transplants. In a previous study conducted by our lab, the same decellularization protocol was applied in human umbilical arteries, where also the elimination of the HLA class I and II antigens was confirmed after the accomplishment of a comprehensive shotgun quantitative proteomic analysis [69]. The above results suggest further that the proposed decellularization protocol successfully produced low immunogenic full-thickness abdominal wall scaffolds derived from Wistar rats. The study presented herein, demonstrated a proof-of-concept protocol for the production of acellular full-thickness abdominal wall scaffolds, for potential use as transplants. In this study, an already established decellularization protocol, which has been validated by our research team in several tissues and organs, including the human umbilical cord artery, Wharton's jelly tissue, oesophagus and kidney, was evaluated for the

proposed tissue [38,52,69–72]. In the past, also other research groups tried to produce full-thickness abdominal wall scaffolds, with contradictory results. Specifically, Chiu *et. al.* [34] demonstrated the production of the porcine acellular dermal matrix (ADM) decellularized with the use of supercritical carbon dioxide ($SCCO_2$). Chiu *et. al.* [34] successfully produced ADM with this method, however, both ECM ultrastructure and main components appeared to be significantly affected by the $SCCO_2$. There was a significant difference between non-decellularized and decellularized samples regarding the histological stain intensity. In addition, ADM samples in higher magnification are characterized by alterations in ECM integrity. On the other hand, in our study, no alteration in histological stain intensity between non-decellularized and decellularized samples (either from 1st, the 2nd or 3rd cycle) was observed. Only sGAG content was affected by the proposed decellularization protocol as it was confirmed by both histological and quantification results. However, in the majority of the studies focused on the production of decellularized scaffolds, a similar loss of sGAGs has been observed [38,49,50,69–72]. Moreover, the sGAG content loss and cellular population elimination are responsible for the altered mechanical properties of the acellular scaffolds. In addition, although the studies conducted by the Buell *et. al.* [33] and Sanchez *et. al.* [32] indicated the production of acellular abdominal wall scaffolds, the tissue ECM was affected in a similar way as in the study of Chiu *et. al.* [34]. Taking into account the available data from the literature, in our study, a comprehensive evaluation of the decellularized scaffold histology (circumferential vs longitudinal axis) was performed, in order to acquire safe conclusions.

In conclusion, the results of this study clearly showed the successful production of a full-thickness rat-derived abdominal wall scaffold. Moreover, major immunogenic epitopes such as the α-gal or the RT1 class I and II antigens were removed, thus the produced scaffolds characterized by low immunogenicity. Considering our results, in the near future a second study is primarily prepared, where implantation of the produced full-thickness decellularized abdominal wall scaffold will be performed in an animal model, in order to investigate deeper the behavior of the transplant in terms of mechanical strength, capability for tissue integration, non-immunogenic nature and also the underlying tissue remodelling mechanisms. The proposed decellularization protocol efficiently could be used for the production of abdominal wall scaffolds derived from large animal models (porcine origin) or human cadaveric donors. Furthermore, this study exploited the possibility of the production of non-immunogenic acellular meshes, with good tissue integrity and mechanical properties, suitable to be used as transplants in abdominal wall defects. The production of such acellular biologic scaffolds, with *in vivo* tissue remodelling properties can be considered superior to the current gold-standard methods (e.g. synthetic scaffolds). Hence comprehensive evaluation of the properties of the decellularized biologic scaffolds is required to be performed in the future, to ensure the appropriate FDA clearance. Under these circumstances, these scaffolds could be used more efficiently by clinicians, bringing them one step closer to their clinical utility.

Author Contributions: Conceptualization, G.S. and P.M., methodology, G.S.; P.M.; E.K.; B.S. and C.P., validation, G.S. and P.M., formal analysis, G.S. and P.M.,, investigation, G.S. and P.M., data curation, P.M. writing—original draft preparation, P.M., writing—review and editing, E.M. and L.P., supervision, E.M.; L.P. and G.T., project administration, G.S. All authors have read and agreed to the published version of the manuscript.

Funding: This research received no external funding.

Institutional Review Board Statement: The study protocol involved the harvest of full-thickness abdominal wall from Wistar Rats (n=30), weighing 300- 350 gr. All care and handling of the animals were provided according to the Guide for the Care and Use of Laboratory Animals of BRFAA, conformed to the Directive 2010/63/EU of the European Parliament, and has been approved by the Bioethics Committee of BRFAA (ref 02-2021).

Informed Consent Statement: Non Applicable.

Data Availability Statement: The data that support the findings of this study are available upon request from the corresponding author, Panagiotis Mallis. The data are not publicly available due to information that could compromise the privacy of patients.

Conflicts of Interest: The authors declare no conflict of interest.

References

1. Meintjes, J.; Yan, S.; Zhou, L.; Zheng, S.; Zheng, M. Synthetic, biological and composite scaffolds for abdominal wall reconstruction. *Expert Rev Med* Devices. **2011**, *8* ,275-88.
2. Hope, W.W.; Abdul, W.; Winters, R. Abdominal Wall Reconstruction. [Updated 2022 Jul 25]. In: StatPearls [Internet]. Treasure Island (FL): StatPearls Publishing; 2022 Jan-. Available from: https://www.ncbi.nlm.nih.gov/books/NBK431108/
3. Kingsnorth, A.; LeBlanc, K. Hernias: inguinal and incisional. *Lancet.* **2003**, *362* ,1561-71.
4. Luijendijk, R.W.; Hop, W.C.; van den Tol, M.P.; de Lange, D.C.; Braaksma, M.M.; IJzermans, J.N.; Boelhouwer, R.U.; de Vries, B.C.; Salu, M.K.; Wereldsma, J.C.; Bruijninckx, C.M.; Jeekel, J. A comparison of suture repair with mesh repair for incisional hernia. *N Engl J Med*. **2000**, *343*, 392-8.
5. Klinge, U.; Si, Z.Y.; Zheng, H; Schumpelick, V; Bhardwaj, R.S; Klosterhalfen, B. Abnormal collagen I to III distribution in the skin of patients with incisional hernia. *Eur Surg Res*. **2000**, *32*, 43-8.
6. Klinge, U.; Zheng, H.; Si, Z.; Schumpelick, V.; Bhardwaj, R.S.; Muys, L.; Klosterhalfen, B. Expression of the extracellular matrix proteins collagen I, collagen III and fibronectin and matrix metalloproteinase-1 and -13 in the skin of patients with inguinal hernia. *Eur Surg Res*. **1999**, *31*, 480-90.
7. Zheng, H.; Si, Z.; Kasperk, R.; Bhardwaj, R.S.; Schumpelick, V.; Klinge, U.; Klosterhalfen, B. Recurrent inguinal hernia: disease of the collagen matrix? *World J Surg*. **2002**, *26* , 401-8.
8. Bringman, S.; Conze, J.; Cuccurullo, D.; Deprest, J.; Junge, K.; Klosterhalfen, B.; Parra-Davila, E.; Ramshaw, B.; Schumpelick, V. Hernia repair: the search for ideal meshes. *Hernia*. **2010**, *14* ,81-7.
9. Cobb, W.S. A Current Review of Synthetic Meshes in Abdominal Wall Reconstruction. *Plast Reconstr Surg.* **2018**, *142*, 64S-71S.
10. Todros, S.; Pavan, P.G.; Natali, A.N. Synthetic surgical meshes used in abdominal wall surgery: Part I-materials and structural conformation. *J Biomed Mater Res B Appl Biomater***. 2017**, *105* ,689-699.
11. Todros, S.; Pavan, P.G.; Pachera, P.; Natali, A.N. Synthetic surgical meshes used in abdominal wall surgery: Part II-Biomechanical aspects. *J Biomed Mater Res B Appl Biomater*. **2017**, *105* ,892-903.
12. Finch, D.; Mehmood, S.; Varghese, J. Abdominal wall reconstruction using biosynthetic absorbable mesh in high-risk complex ventral hernia. *Swiss Med Wkly*. **2021**, *151*, w20449.
13. Fatkhudinov, T.; Tsedik, L.; Arutyunyan. I.; Lokhonina, A.; Makarov, A.; Korshunov, A.; Elchaninov, A.; Kananykhina, E.; Vasyukova, O.; Usman, N.; Uvarova E, Chuprynin V, Eremina I, Degtyarev D, Sukhikh G. Evaluation of resorbable polydioxanone and polyglycolic acid meshes in a rat model of ventral hernia repair. *J Biomed Mater Res B Appl Biomater*. **2019**, *107*, 652-663.
14. Baumann, D.P.; Butler, C.E. Bioprosthetic mesh in abdominal wall reconstruction. *Semin Plast Surg*. **2012**, *26* ,18-24.
15. Rahimnejad, M.; Derakhshanfar, S.; Zhong, W.; Biomaterials and tissue engineering for scar management in wound care. *Burns Trauma*. **2017**, *5* ,4.
16. Wissing, T.B.; Bonito, V.; van Haaften, E.E.; van Doeselaar, M.; Brugmans, MMCP.; Janssen, H.M.; Bouten, C.V.C.; Smits, AIPM. Macrophage-Driven Biomaterial Degradation Depends on Scaffold Microarchitecture**.** *Front Bioeng Biotechnol*. **2019**, *7* ,87.
17. Saleh, L.S.; Bryant, S.J. The Host Response in Tissue Engineering: Crosstalk Between Immune cells and Cell-laden Scaffolds. *Curr Opin Biomed Eng*. **2018** , *6* ,58-65.
18. Deeken, C.R.; Lake, S.P. Mechanical properties of the abdominal wall and biomaterials utilized for hernia repair. *J Mech Behav Biomed Mater*. **2017**, *74* , 411-427.
19. Nisiewicz, M.; Hughes, T.; Plymale, M.A.; Davenport, D.L.; Roth, J.S. Abdominal wall reconstruction with large polypropylene mesh: is bigger better? *Hernia.* **2019**, *23* ,1003-1008.
20. Gui, D.; Spada, P.L.; Di, Mugno, M.; Sermoneta, D.; Runfola, M.; Rossi, S. Abdominal wall closure with ePTFE--Goretex Dual Mesh after detensive laparotomy for abdominal compartment syndrome. *Acta Biomed*. **2003**, *74* Suppl 2, 51-4.
21. Ünek, T.; Sökmen, S.; Egeli, T.; Avkan Oğuz, V.; Ellidokuz, H.; Obuz, F. The results of expanded-polytetrafluoroethylene mesh repair in difficult abdominal wall defects. *Asian J Surg.* **2019**, *42* ,131-143.
22. Bellows, C.F.; Alder, A.; Helton, W.S. Abdominal wall reconstruction using biological tissue grafts: present status and future opportunities. *Expert Rev Med Devices*. **2006**, *3* ,657-75.

23. Costa, A.; Adamo, S.; Gossetti, F.; D'Amore, L.; Ceci, F.; Negro, P.; Bruzzone, P. Biological Scaffolds for Abdominal Wall Repair: Future in Clinical Application? *Materials (Basel).* **2019**, *12* ,2375.
24. Dixit, S.; Baganizi, D.R.; Sahu, R.; Dosunmu, E.; Chaudhari, A.; Vig, K.; Pillai, S.R.; Singh SR, Dennis VA. Immunological challenges associated with artificial skin grafts: available solutions and stem cells in future design of synthetic skin. *J Biol Eng.* 2017, *13* ,11-49.
25. Velnar, T.; Bunc, G.; Klobucar, R.; Gradisnik, L. Biomaterials and host versus graft response: a short review. *Bosn J Basic Med Sci.* **2016**, *16* , 82-90.
26. de Castro Brás, L.E.; Shurey, S.; Sibbons, P.D. Evaluation of crosslinked and non-crosslinked biologic prostheses for abdominal hernia repair. *Hernia*. **2012** ,*16* ,77-89.
27. Mallis, P.; Kostakis, A.; Stavropoulos-Giokas, C.; Michalopoulos, E. Future Perspectives in Small-Diameter Vascular Graft Engineering. *Bioengineering (Basel)*. **2020**, *7* ,160.
28. Gilbert, T.W.; Sellaro, T.L.; Badylak, S.F. Decellularization of tissues and organs. *Biomaterials*. **2006**, *27*, 675-83.
29. Porzionato, A.; Stocco, E.; Barbon, S.; Grandi, F.; Macchi, V.; De Caro, R. Tissue-Engineered Grafts from Human Decellularized Extracellular Matrices: A Systematic Review and Future Perspectives. *Int J Mol Sci*. **2018**, *19*, 4117.
30. Zhang, X.; Chen, X.; Hong, H.; Hu, R.; Liu, J.; Liu, C. Decellularized extracellular matrix scaffolds: Recent trends and emerging strategies in tissue engineering. *Bioact Mater*. **2021**, *10* , 15-31.
31. Parmaksiz, M.; Dogan, A.; Odabas, S.; Elçin, A.E.; Elçin, Y.M. Clinical applications of decellularized extracellular matrices for tissue engineering and regenerative medicine. *Biomed Mater.* **2016**, *11* ,022003.
32. Sánchez, J.C.; Díaz, D.M.; Sánchez, L.V.; Valencia-Vásquez, A.; Quintero, J.F.; Muñoz, L.V.; Bernal, A.F.; Osorio, G.; Guerra, Á.; Buitrago, J. Decellularization and In Vivo Recellularization of Abdominal Porcine Fascial Tissue. *Tissue Eng Regen Med***. 2021**, *18* ,369-376.
33. Buell, J.F.; Helm, J.; Mckillop, I.H.; Iglesias, B.; Pashos, N.; Hooper, P. Decellularized biologic muscle-fascia abdominal wall scaffold graft. *Surgery.* **2021**, *169* ,595-602.
34. Chiu, Y.L.; Lin, Y.N.; Chen, Y.J.; Periasamy, S, Yen, K.C.; Hsieh, D.J. Efficacy of Supercritical Fluid Decellularized Porcine Acellular Dermal Matrix in the Post-Repair of Full-Thickness Abdominal Wall Defects in the Rabbit Hernia Model. *Processes*. **2022**, *10*, 2588.
35. Guyette, J.P.; Gilpin, S.E.; Charest, J.M.; Tapias, L.F.; Ren, X.; Ott, H.C. Perfusion decellularization of whole organs. *Nat Protoc*. **2014**, *9* ,1451-68.
36. Mallis, P.; Oikonomidis, C.; Dimou, Z.; Stavropoulos-Giokas, C.; Michalopoulos, E.; Katsimpoulas, M. Optimizing Decellularization Strategies for the Efficient Production of Whole Rat Kidney Scaffolds. *Tissue Eng Regen Med*. **2021** ,*18* ,623-640.
37. Schmitt, A.; Csiki, R.; Tron, A.; Saldamli, B.; Tübel, J.; Florian, K.; Siebenlist, S.; Balmayor, E.; Burgkart, R. Optimized protocol for whole organ decellularization. *Eur J Med Res*. **2017**, *22* ,31.
38. Gelse, K.; Poschl, E.; Aigner, T. Collagens—Structure, function, and biosynthesis. *Adv. Drug Deliv. Rev*. **2003**, *55*, 1531–1546.
39. Bellis, S.L. Advantages of RGD peptides for directing cell association with biomaterials. **Biomaterials. 2011**, *32* ,4205-10.
40. Davidenko, N.; Schuster, C.F.; Bax, D.V.; Farndale. R.W.; Hamaia. S.; Best, S.M.; Cameron, R.E.Evaluation of cell binding to collagen and gelatin: a study of the effect of 2D and 3D architecture and surface chemistry. *J Mater Sci: Mater Med* **2016**, *27* , 148.
41. Taubenberger, A.V.; Woodruff, M.A.; Bai, H.; Muller, D.J.; Hutmacher, D.W. The effect of unlocking RGD-motifs in collagen I on pre-osteoblast adhesion and differentiation. *Biomaterials*. **2010**, *31* ,2827-35.
42. Gullberg, D.E.; Lundgren-Akerlund, E. Collagen-binding I domain integrins--what do they do? *Prog Histochem Cytochem*. **2002**, *37* ,3-54.
43. Murphy, C.M.; Duffy, G.P.; Schindeler, A.; O'brien, F.J. Effect of collagen-glycosaminoglycan scaffold pore size on matrix mineralization and cellular behavior in different cell types. *J Biomed Mater Res A.* **2016**, *104*, 291-304.
44. Boraschi, D.I.; Wang, J.; Mort, J.S.; Komatova, S.V. Collagen Type I as a Ligand for Receptor-Mediated Signaling. *Frontiers in Physics.* **2017**, *5* ,1-11.
45. Shishido, S.; Bönig, H.; Kim, Y.M. Role of integrin alpha4 in drug resistance of leukemia. *Front Oncol.* **2014**, *4* , 99.

46. Hou, S.; Wang, J.; Li, W.; Hao, X.; Hang, Q. Roles of Integrins in Gastrointestinal Cancer Metastasis. *Front Mol Biosci*. **2021** , *8* ,708779.
47. Junqueira, L.C.; Montes, G.S. Biology of collagen-proteoglycan interaction. *Arch Histol Jpn*. **1983** ,*46* ,589-629.
48. Mattson, J.M.; Turcotte, R.; Zhang, Y. Glycosaminoglycans contribute to extracellular matrix fiber recruitment and arterial wall mechanics. *Biomech Model Mechanobiol*. **2017**, *16* ,213-225.
49. Luo, J.; Korossis, S.A.; Wilshaw, S.P.; Jennings. L.M.; Fisher, J.; Ingham, E. Development and characterization of acellular porcine pulmonary valve scaffolds for tissue engineering. *Tissue Eng Part A*. **2014**, *20* ,2963–2974.
50. Gui, L.; Muto, A.; Chan, S.A.; Breuer, C.K.; Niklason, L.E. Development of decellularized human umbilical arteries as small-diameter vascular grafts. *Tissue Eng Part A*. **2009**, *15* ,2665–2676.
51. Crapo, P.M.; Gilbert, T.W.; Badylak, S.F. An overview of tissue and whole organ decellularization processes. *Biomaterials*. **2011**, *32* ,3233-43.
52. Mallis, P.; Katsimpoulas, M.; Kostakis, A.; Dipresa, D.; Korossis, S.; Papapanagiotou, A.; Kassi, E.; Stavropoulos-Giokas, C.; Michalopoulos, E. Vitrified Human Umbilical Arteries as Potential Grafts for Vascular Tissue Engineering. *Tissue Eng Regen Med.* **2020**, *17* ,285-299.
53. Arai, S.; Lacerda, C.; Orton ,E.C. Tissue-gel electrophoresis enhances antigen removal from porcine aortic valve and bovine pericardium. *J Heart Valve Dis*. **2010**, *19* ,753-8.
54. Korhonen, R.K.; Julkunen, P.; Wilson, W.; Herzog. W. Importance of collagen orientation and depth-dependent fixed charge densities of cartilage on mechanical behavior of chondrocytes. *J Biomech Eng*. **2008**, *130* ,021003.
55. Sexton, A.J.; Turmaine, M.; Cai, W.Q.; Burnstock, G. A study of the ultrastructure of developing human umbilical vessels. *J. Anat.* **1996** ,*188* ,75–85.
56. Stehbens, W.E.; Wakefield, J.S.; Gilbert-Barness, E.; Zuccollo, J.M. Histopathology and ultrastructure of human umbilical blood vessels. *Fetal Pediatr. Pathol*. **2005**, *24* ,297–315.
57. Sassani, S.G.; Tsangaris, S.; Sokolis, D.P. Layer- and region-specific material characterization of ascending thoracic aortic aneurysms by microstructure-based models. *J Biomech.* **2015**, *48* ,3757-65.
58. Roy, S.; Silacci, P.; Stergiopulos, N. Biomechanical properties of decellularized porcine common carotid arteries. *Am J Physiol Heart Circ Physiol*. **2005** ,*289* ,H1567-76.
59. Galili, U. Biosynthesis of α-Gal Epitopes (Galα1-3Galβ1-4GlcNAc-R) and Their Unique Potential in Future α-Gal Therapies. *Front Mol Biosci*. **2021**, *8*, 746883.
60. Galili, U. Anti-Gal: an abundant human natural antibody of multiple pathogeneses and clinical benefits. *Immunology*. **2013**, *140* ,1-11.
61. Ekser, B.; Cooper, D.K. Overcoming the barriers to xenotransplantation: prospects for the future. *Expert Rev Clin Immunol*. **2010**, *6* , 219-30.
62. Zhong, R. Gal knockout and beyond. *Am J Transplant*. **2007**, *7*, 5-11.
63. Milland, J.; Christiansen, D.; Sandrin, M.S. Alpha1,3-galactosyltransferase knockout pigs are available for xenotransplantation: are glycosyltransferases still relevant? *Immunol Cell Biol*. **2005**, *83* ,687-93.
64. Wu, L.C.; Kuo, Y.J.; Sun, F.W.; Chen, C.H.; Chiang, C.J.; Weng, P.W.; Tsuang, Y.H.; Huang, Y.Y. Optimized decellularization protocol including α-Gal epitope reduction for fabrication of an acellular porcine annulus fibrosus scaffold. *Cell Tissue Bank*. **2017**, *18*, 383-396.
65. Kasravi, M.; Ahmadi, A.; Babajani, A.; Mazloomnejad, R.; Hatamnejad, M.R.; Shariatzadeh, S.; Bahrami, S.; Niknejad, H. Immunogenicity of decellularized extracellular matrix scaffolds: a bottleneck in tissue engineering and regenerative medicine. *Biomater Res*. **2023**, *27* ,10.
66. Joziasse, D.H.; Oriol, R. Xenotransplantation: the importance of the Galalpha1,3Gal epitope in hyperacute vascular rejection. *Biochim Biophys Acta*. 1999, *1455* , 403-18.
67. Günther, E.; Walter, L. The major histocompatibility complex of the rat (Rattus norvegicus). *Immunogenetics*. **2001**, *53*, 520-42.
68. Walter, L.; Hurt, P.; Himmelbauer, H.; Sudbrak, R.; Günther, E. Physical mapping of the major histocompatibility complex class II and class III regions of the rat. *Immunogenetics*. **2002**, *54*, 268-75.
69. Mallis, P.; Sokolis, D.P.; Makridakis, M.; Zoidakis, J.; Velentzas, A.D.; Katsimpoulas, M.; Vlahou, A.; Kostakis, A, Stavropoulos-Giokas C, Michalopoulos E. Insights into Biomechanical and Proteomic Characteristics of Small Diameter Vascular Grafts Utilizing the Human Umbilical Artery. *Biomedicines*. **2020**, *8* , 280.

70. Mallis, P.; Chachlaki, P.; Katsimpoulas, M.; Stavropoulos-Giokas, C.; Michalopoulos, E. Optimization of Decellularization Procedure in Rat Esophagus for Possible Development of a Tissue Engineered Construct. *Bioengineering (Basel).* **2018**, *6*, 3.
71. Mallis, P.; Boulari, D.; Chachlaki, P.; Stavropoulos Giokas, C.; Michalopoulos E. Vitrified Wharton's jelly tissue as a biomaterial for multiple tissue engineering applications. *Gynecol Endocrinol*. **2020**, *36,* 139-142.
72. Mallis, P.; Boulari, D.; Michalopoulos, E.; Dinou, A.; Spyropoulou-Vlachou, M.; Stavropoulos-Giokas, C. Evaluation of HLA-G Expression in Multipotent Mesenchymal Stromal Cells Derived from Vitrified Wharton's Jelly Tissue. *Bioengineering (Basel).* **2018**, *5* , 95.